C Journal of Carbon Research

MDPI

Article

Casimir–Polder Force on Atoms or Nanoparticles from Gapped and Doped Graphene: Asymptotic Behavior at Large Separations

Galina L. Klimchitskaya [1,2] and Vladimir M. Mostepanenko [1,2,3,*]

[1] Central Astronomical Observatory at Pulkovo of the Russian Academy of Sciences, 196140 Saint Petersburg, Russia
[2] Peter the Great Saint Petersburg Polytechnic University, 195251 Saint Petersburg, Russia
[3] Kazan Federal University, 420008 Kazan, Russia
* Correspondence: vmostepa@gmail.com

Abstract: The Casimir–Polder force acting on atoms and nanoparticles spaced at large separations from real graphene sheets possessing some energy gaps and chemical potentials is investigated in the framework of the Lifshitz theory. The reflection coefficients expressed via the polarization tensor of graphene, found based on the first principles of thermal quantum field theory, are used. It is shown that for graphene the separation distances, starting from which the zero-frequency term of the Lifshitz formula contributes more than 99% of the total Casimir–Polder force, are less than the standard thermal length. According to our results, however, the classical limit for graphene, where the force becomes independent of the Planck constant, may be reached at much larger separations than the limit of the large separations determined by the zero-frequency term of the Lifshitz formula, depending on the values of the energy gap and chemical potential. The analytic asymptotic expressions for the zero-frequency term of the Lifshitz formula at large separations are derived. These asymptotic expressions agree up to 1% with the results of numerical computations starting from some separation distances that increase with increasing energy gaps and decrease with increasing chemical potentials. The possible applications of the obtained results are discussed.

Keywords: Casimir–Polder force; atoms; nanoparticles; Lifshitz theory; graphene; polarization tensor; energy gap; chemical potential

Citation: Klimchitskaya, G.L.; Mostepanenko, V.M. Casimir–Polder Force on Atoms or Nanoparticles from Gapped and Doped Graphene: Asymptotic Behavior at Large Separations. *C* **2023**, *9*, 64. https://doi.org/10.3390/c9030064

Academic Editors: Matteo Strozzi and Ahmet Sinan Oktem

Received: 30 May 2023
Revised: 16 June 2023
Accepted: 25 June 2023
Published: 4 July 2023

1. Introduction

The Casimir–Polder force [1] acts between electrically neutral small bodies (atoms and nanoparticles) and material surfaces. This force is induced by the zero-point and thermal fluctuations of the electromagnetic field, which have their origin in the microscopic charges and currents occurring inside all material bodies. It is a generalization of the van der Waals force to separation distances, where the relativistic effects already make a pronounced impact on the force value. This typically happens at separations exceeding several nanometers.

The unified theory of the atom–plate van der Waals and Casimir–Polder forces was developed by Lifshitz [2–4]. Given the dynamic polarizability, $\alpha(\omega)$, of an atom or a nanoparticle and the dielectric function of a material plate, one can calculate the Casimir–Polder force in the framework of the Lifshitz theory. Calculations of this kind have been performed for different atoms, nanoparticles, and plate materials [5–20]. The obtained results were found to be important in explaining the crucially new physical phenomena of quantum reflection [21–30] and Bose–Einstein condensation [31–35]. It should be noted that the original Lifshitz theory was formulated for physical systems that are in a state of thermal equilibrium with the environment. The generalization of this theory for situations out of thermal equilibrium (for instance, when the plate temperature is different from that of the

environment) has been performed in [36–41]. It was applied to calculate the nonequilibrium Casimir–Polder force in different cases, including experimental configurations [42–45].

Considerable attention has recently been focused on graphene, which is a two-dimensional sheet of carbon atoms packed in a hexagonal lattice [46]. Currently, graphene finds expanding applications in both fundamental physics and nanotechnology. Specifically, the Casimir–Polder force acting on atoms [47–59] and nanoparticles [60–65] from graphene and graphene-coated substrates has become the topic of a large body of research. Graphene was demonstrated to have properties described by the Dirac model [46,66,67], i.e., at energies below approximately 3 eV [68] electrons in graphene can be considered as a set of massless or light quasiparticles governed by the Dirac equation in two spatial dimensions, where the speed of light, c, is replaced by the Fermi velocity, $v_F \approx c/300$. This has made it possible to find the polarization tensor of graphene at any temperature [69–72], which is equivalent to spatially nonlocal dielectric functions, transverse one and longitudinal one. These results have been used in [48–51,53–59,65] to calculate the Casimir–Polder force acting on an atom or a nanoparticle from graphene in the framework of the Lifshitz theory.

An important question is how soon the Casimir–Polder force from graphene approaches its limiting form, given by the zero-frequency term in the Lifshitz formula, which can be reached at large separations (high temperatures). In [73], the asymptotic behavior of the Casimir–Polder interaction was investigated in the case of an undoped graphene sheet possessing zero chemical potential. However, real graphene sheets are characterized not only by the energy gap in the spectrum of quasiparticles, $\Delta = 2mv_F^2$, where m is the small but nonzero mass of quasiparticles [46,74,75], but they are also doped, i.e., their crystal lattice contains some fraction of foreign atoms. This can be described by a nonzero value of the chemical potential, μ, depending on the doping concentration [76].

In this article, we examine the behavior of the Casimir–Polder force between atoms (nanoparticles) and real graphene sheets in the limit of large separations (high temperatures) as a function of the atom–plate separation a, the energy gap Δ, and the chemical potential μ. First, we demonstrate that the term of the Lifshitz formula at zero Matsubara frequency contributes more than 99% of the force magnitude at separations exceeding some value a_0, which is distinctly less than the standard thermal length, $\hbar c/k_B T) \approx 7.6$ μm at room temperature, $T = 300$ K (here, k_B is the Boltzmann constant). The value of a_0 decreases with increasing Δ. For sufficiently small Δ, a_0 increases with increasing μ, but for a larger Δ the dependence of a_0 on μ becomes nonmonotonic.

Then, we compare the large-separation Casimir–Polder force from graphene, given by the zero-frequency term of the Lifshitz formula, with that from an ideal metal plane. It is shown that for a fixed energy gap an agreement between these two quantities becomes better with increasing chemical potential of a graphene sheet.

Next, we derive simple asymptotic expressions for the zero-frequency contribution to the Lifshitz formula at large separations and find how they agree with the results of numerical computations. For this purpose, we use the zero-frequency term of the Lifshitz formula with reflection coefficients expressed via the polarization tensor of graphene. The polarization tensor is calculated using several small parameters. The analytic asymptotic expressions for the large-separation Casimir–Polder force are derived for any values of the energy gap and chemical potential of a graphene sheet.

The derived asymptotic expressions are compared with numerical computations of the Casimir–Polder force at large separations. The application region of the analytic asymptotic results is determined. We show that with increasing energy gap the agreement between the asymptotic and computational results becomes worse, whereas, at the same separation, an increase in the chemical potential brings the asymptotic results in better agreement with the results of numerical computations.

This article is organized as follows: In Section 2, we present the Lifshitz formula for the Casimir–Polder force and reflection coefficients for the case of gapped and doped graphene in terms of the polarization tensor. Section 3 contains the exact expression and numerical computations of the Casimir–Polder force at large separations. In Section 4,

the analytic asymptotic expressions for the Casimir–Polder force are derived. In Section 5, the asymptotic results for the Casimir–Polder force are compared with the results of numerical computations. Section 6 contains a discussion, and Section 7 contains our conclusions.

2. The Lifshitz Formula and Reflection Coefficients for Gapped and Doped Graphene

The Casimir–Polder force between an atom or a nanoparticle and any plane surface is expressed by the following Lifshitz formula, which we present in terms of dimensionless variables [54,77]:

$$F(a,T)=-\frac{k_BT}{8a^4}{\sum_{l=0}^{\infty}}'\alpha_l\int_{\zeta_l}^{\infty}y\,dy\,e^{-y}\Big[(2y^2-\zeta_l^2)r_{\rm TM}(i\zeta_l,y)-\zeta_l^2r_{\rm TE}(i\zeta_l,y)\Big]. \tag{1}$$

Here, the prime on the sum in l means that the term with $l=0$ is divided by 2, $\zeta_l=\xi_l/\omega_c$, where $\xi_l=2\pi k_BTl/\hbar$ ($l=0,\,1,\,2,\,\ldots$) are the Matsubara frequencies, $\omega_c=c/(2a)$ is the characteristic frequency, and $\alpha_l=\alpha(i\zeta_l\omega_c)$. The dimensionless variable y is defined as

$$y=2aq_l=2a\left(k_\perp^2+\frac{\xi_l^2}{c^2}\right)^{1/2}, \tag{2}$$

where $k_\perp$ is the magnitude of the wave vector projection on the plane of graphene, and $r_{\rm TM,TE}$ are the reflection coefficients on graphene for the transverse magnetic (p) and transverse electric (s) polarizations of the electromagnetic field. Note that both the dynamic polarizability, α_l, and the reflection coefficients, $r_{\rm TM,TE}$, are calculated at the pure imaginary frequencies $i\zeta_l$.

The reflection coefficients in (1) are expressed via the dimensionless polarization tensor of graphene [54]

$$r_{\rm TM}(i\zeta_l,y)=\frac{y\widetilde{\Pi}_{00,l}}{y\widetilde{\Pi}_{00,l}+2(y^2-\zeta_l^2)},\qquad r_{\rm TE}(i\zeta_l,y)=-\frac{\widetilde{\Pi}_l}{\widetilde{\Pi}_l+2y(y^2-\zeta_l^2)}, \tag{3}$$

where the components of the dimensionless $\widetilde{\Pi}_{\beta\gamma}$ and dimensional $\Pi_{\beta\gamma}$ tensors ($\beta,\gamma=0,\,1,\,2$) are connected by

$$\widetilde{\Pi}_{\beta\gamma,l}\equiv\widetilde{\Pi}_{\beta\gamma}(i\zeta_l.y)=\frac{2a}{\hbar}\Pi_{\beta\gamma}(i\xi_l,k_\perp). \tag{4}$$

The dimensionless quantity $\widetilde{\Pi}_l$ in (2) is defined as

$$\widetilde{\Pi}_l\equiv\frac{(2a)^3}{\hbar}(k_\perp^2\Pi_{\beta,l}^{\beta}-q_l^2\Pi_{00.l})=(y^2-\zeta_l^2)\widetilde{\Pi}_{\beta,l}^{\beta}-y^2\widetilde{\Pi}_{00.l} \tag{5}$$

with a summation over β. The arguments of the polarization tensor components are omitted for brevity.

As mentioned in the Introduction, the polarization tensor of graphene is equivalent to the spatially nonlocal transverse and longitudinal dielectric functions defined in two-dimensional space [78,79]. Using the dimensionless variables, one obtains

$$\varepsilon^{\rm L}(i\zeta_l,y)=1+\frac{1}{2\sqrt{y^2-\zeta_l^2}}\widetilde{\Pi}_{00,l},\qquad \varepsilon^{\rm Tr}(i\zeta_l,y)=1+\frac{1}{2\zeta_l^2\sqrt{y^2-\zeta_l^2}}\widetilde{\Pi}_l. \tag{6}$$

The explicit expression for $\widetilde{\Pi}_{00,l}$ in terms of the dimensionless variables ζ_l and y is presented in [54]. After identical transformations, it can be put in a more convenient form

$$\widetilde{\Pi}_{00,l}=\alpha\frac{y^2-\zeta_l^2}{p_l}\Psi(D_l)+\frac{16\alpha a k_BT}{\tilde{v}_F^2\hbar c}\ln\left[\left(e^{-\frac{\Delta}{2k_BT}}+e^{\frac{\mu}{k_BT}}\right)\left(e^{-\frac{\Delta}{2k_BT}}+e^{-\frac{\mu}{k_BT}}\right)\right]$$
$$-\frac{4\alpha p_l}{\tilde{v}_F^2}\int\limits_{D_l}^{\infty}du\,w_l(u,y)\,\mathrm{Re}\frac{p_l-p_lu^2+2i\zeta_lu}{[p_l^2-p_l^2u^2+\tilde{v}_F^2(y^2-\zeta_l^2)D_l^2+2i\zeta_lp_lu]^{1/2}}. \tag{7}$$

Here, $\alpha=e^2/(\hbar c)$ is the fine structure constant,

$$\Psi(x)=2\left[x+(1-x^2)\mathrm{arctan}\frac{1}{x}\right],\qquad p_l=\sqrt{\tilde{v}_F^2y^2+(1-\tilde{v}_F^2)\zeta_l^2}, \tag{8}$$

where $\tilde{v}_F=v_F/c$ is the dimensionless Fermi velocity,

$$w_l(u,y)=\frac{1}{e^{B_lu+\frac{\mu}{k_BT}}+1}+\frac{1}{e^{B_lu-\frac{\mu}{k_BT}}+1} \tag{9}$$

and, finally,

$$D_l\equiv D_l(y)=\frac{2a\Delta}{\hbar cp_l},\qquad B_l\equiv B_l(y)=\frac{\hbar cp_l}{4ak_BT}. \tag{10}$$

In a similar way, the combination of the components of the polarization tensor $\widetilde{\Pi}_l$ entering Equation (3) can be written in the form [54]

$$\widetilde{\Pi}_l=\alpha(y^2-\zeta_l^2)p_l\Psi(D_l)-\frac{16\alpha a k_BT\zeta_l^2}{\tilde{v}_F^2\hbar c}\ln\left[\left(e^{-\frac{\Delta}{2k_BT}}+e^{\frac{\mu}{k_BT}}\right)\left(e^{-\frac{\Delta}{2k_BT}}+e^{-\frac{\mu}{k_BT}}\right)\right]$$
$$+\frac{4\alpha p_l^2}{\tilde{v}_F^2}\int\limits_{D_l}^{\infty}du\,w_l(u,y)\,\mathrm{Re}\frac{\zeta_l^2-p_l^2u^2+\tilde{v}_F^2(y^2-\zeta_l^2)D_l^2+2i\zeta_lp_lu}{[p_l^2-p_l^2u^2+\tilde{v}_F^2(y^2-\zeta_l^2)D_l^2+2i\zeta_lp_lu]^{1/2}}. \tag{11}$$

By using Equations (1), (3), (7) and (11), one can compute the Casimir–Polder force between an atom or a nanoparticle and a real graphene sheet characterized by some energy gap and chemical potential.

3. The Casimir–Polder Force at Large Separations

It is well known that at large separations or, equivalently, at high temperatures, the dominant contribution to the Casimir–Polder force is given by the term of (1) with $l=0$ [77,80]. For atoms and nanoparticles interacting with the three-dimensional plates made of ordinary materials, the zero-frequency term of the Lifshitz formula is approximately equal to the total force already at the thermal length, $\hbar c/(k_BT)\approx 7.6$ μm, at room temperature. Below we demonstrate that for graphene the zero-frequency term determines the total force value at even smaller separations depending on the energy gap Δ and chemical potential μ.

The zero-frequency term of the Lifshitz formula is obtained by separating the component with $l=0$ from (1)

$$F_0(a,T)=-\frac{k_BT}{8a^4}\alpha_0\int\limits_0^{\infty}y^3dy\,e^{-y}r_{\mathrm{TM}}(0,y), \tag{12}$$

where the reflection coefficient from (3) simplifies to

$$r_{\rm TM}(0,y)=\frac{\widetilde{\Pi}_{00,0}(y)}{\widetilde{\Pi}_{00,0}(y)+2y}. \tag{13}$$

Note that the TE reflection coefficient does not contribute to (12) because in (1) taken at $l=0$ it is multiplied by zero. Here, we have explicitly indicated the argument y of the polarization tensor. The component of the dimensionless polarization tensor $\widetilde{\Pi}_{00,0}$ is obtained from (7) by putting $\zeta_0=0$

$$\widetilde{\Pi}_{00,0}(y)=\frac{\alpha y^2}{\tilde{v}_F}\Psi(D_0)+\frac{16\alpha a k_BT}{\tilde{v}_F^2\hbar c}\ln\left[\left(e^{-\frac{\Delta}{2k_BT}}+e^{\frac{\mu}{k_BT}}\right)\left(e^{-\frac{\Delta}{2k_BT}}+e^{-\frac{\mu}{k_BT}}\right)\right] \tag{14}$$
$$-\frac{4\alpha y}{\tilde{v}_F}\int\limits_{D_0}^{\sqrt{1+D_0^2}}du\,w_0(u,y)\,\frac{1-u^2}{\sqrt{1-u^2+D_0^2}},$$

where

$$D_0=\frac{2a\Delta}{\hbar c\tilde{v}_F y}, \qquad B_0=\frac{\hbar c\tilde{v}_F y}{4ak_BT} \tag{15}$$

and $w_0(u,y)$ is defined in (9) with $l=0$ and B_0 from (15).

Here, we perform numerical computations in order to find such separation, a_0, that at all separations $a\geqslant a_0$ the quantity F_0 from (12) contributes no less than 99% of the total Casimir–Polder force (1). This is performed for heavy atoms, for instance, Rb, and nanoparticles. It is apparent that the value of a_0 depends on the energy gap and chemical potential of the specific graphene sheet, so that $a_0=a_0(\Delta,\mu)$. For this purpose, first, we compute F_0 from (12) as a function of separation using Equations (13)–(15). All computations here and below are performed at room temperature, $T=300$ K, in the range of Δ from 0.001 eV to 0.2 eV with a step of 0.01 eV for four values of $\mu=0$, 25, 75, and 150 meV. Similar computations of the total Casimir–Polder force F from (1) are performed by Equations (1), (3), (7), and (11) at separations exceeding 1 μm, where, without the loss of accuracy, one can use an approximation of the static atomic polarizability $\alpha_l\approx\alpha(0)=\alpha_0$ [77]. The point is that computations of the Casimir–Polder force from graphene by (1) using the frequency-dependent polarizability $\alpha(\omega)$ show [54] that even for light atoms, such as He^*, the value of a_0 is above 1 μm. In doing so, for heavy atoms, such as Rb, and nanoparticles all α_l providing contributions to the result (i.e., with $l\leq 6$ at $a=1$ μm, $l\leq 3$ at $a=2$ μm, and $l\leq 2$ at $a=3$ μm) are approximately equal to α_0.

Using the obtained computational results, in Figure 1 we plot a_0 as a function of the energy gap of graphene, Δ, by the four lines (black, red, blue, and brown) for the chemical potential, μ , equal to 0, 25, 75, and 150 meV, respectively. From Figure 1, it can be seen that the value of a_0 decreases with increasing energy gap. For $\Delta<0.15$ eV, the value of a_0 increases with increasing μ, but for larger Δ this is already not the case. Specifically, the value of a_0 for a graphene sheet with $\mu=0$ may become larger than for sheets with $\mu=25$ and 75 meV. Intuitively, it is clear that increasing μ brings graphene closer to an ideal metal and, thus, leads to an increase in a_0. To the contrary, an increase in Δ results in decreasing a_0 due to the suppressed impact of the thermal effects on the Matsubara terms in (1) with $l\geq 1$. The actual value of a_0 for small μ and large Δ results from the interplay between these two effects. By and large, the value of a_0 for gapped and doped graphene is distinctly less than the thermal length for ordinary materials equal to 7.6 μm.

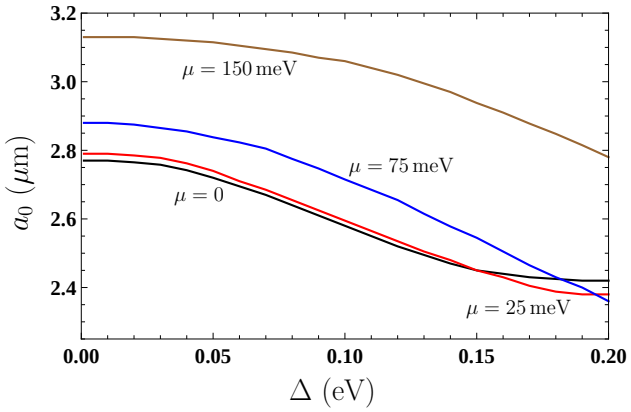

Figure 1. Minimum separation between an atom (nanoparticle) and real graphene sheet for which the zero-frequency term of the Lifshitz formula contributes no less than 99% of the total Casimir–Polder force at $T = 300$ K is shown as a function of the energy gap by the four lines for chemical potential equal to 0, 25, 75, and 150 meV.

It is also interesting to compare the Casimir–Polder force from gapped and doped graphene F_0 at large separations with that from an ideal metal plane given by [77]

$$F_0^{\rm IM}(a,T) = -\frac{3k_BT}{4a^4}\alpha_0. \tag{16}$$

This is the so-called classical limit because the force does not depend on the Planck constant.

To understand where the large-separation Casimir–Polder forces from graphene and an ideal metal plane come together, we compute the relative quantity

$$\delta F_0(a,T) = \frac{F_0(a,T) - F_0^{\rm IM}(a,T)}{F_0^{\rm IM}(a,T)}. \tag{17}$$

The computational results for a graphene sheet with $\Delta = 0.2$ eV are shown in Figure 2 at $T = 300$ K as a function of separation by the four lines (black, red, blue, and brown) from bottom to top for chemical potential μ equal to 0, 25, 75, and 150 meV, respectively. In the inset, the behavior of blue and brown lines at short separations ($\mu = 75$ and 150 eV) is shown on an enlarged scale with better resolution. The dashed lines indicate the border of the 1-percent relative deviation between the large-separation behavior of the Casimir–Polder forces from a graphene sheet and an ideal metal plane. The separation region $a \geqslant 3$ μm is considered where, according to Figure 1, F_0 represents the large-separation behavior of the Casimir–Polder force.

As can be seen in Figure 2, for $\Delta = 0.2$ eV, $\mu = 150$ meV (the top line) the Casimir–Polder forces from graphene and from an ideal metal plane agree within 1% at all separations considered. With decreasing μ to 75, 25, and 0 meV, the agreement within 1% occurs at separations exceeding 7, 36, and 54 μm, respectively. This result is physically natural if one takes into account that larger μ corresponds to larger doping concentrations, i.e., graphene becomes more akin to an ideal metal plane. Thus, for graphene sheets with relatively low chemical potential, the classical limit is reached only at rather large separation distances.

In the next section, we obtain simple asymptotic expressions for the quantity F_0 from (12), which allow the calculation of the Casimir–Polder force from gapped and doped graphene at large separations, without using complicated expressions for the polarization tensor.

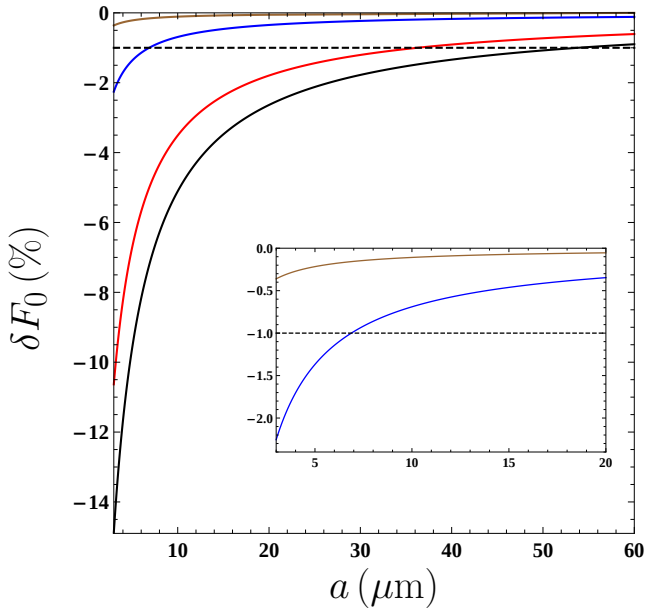

Figure 2. The relative deviation between the high-separation behaviors of the Casimir–Polder force from graphene sheet with $\Delta = 0.2$ eV and an ideal metal plane at $T = 300$ K is shown as a function of the energy gap by the four lines counted from bottom to top for chemical potential equal to 0, 25, 75, and 150 meV. In the inset, the two lines for $\mu = 75$ and 150 meV (bottom and top, respectively) are shown at short separations on an enlarged scale. The dashed lines indicate the border of the 1-percent relative deviation.

4. Asymptotic Expressions for the Casimir–Polder Force

We consider the Casimir–Polder force (12) where the reflection coefficient, r_{TM}, is given by (13) and the polarization tensor is expressed by (14) with the notations in (15). We seek the asymptotic expression of (14) and (12) under the following condition:

$$\frac{2ak_BT}{\tilde{v}_F\hbar c} = \frac{k_BT}{\tilde{v}_F\hbar\omega_c} \gg 1. \tag{18}$$

At $T = 300$ K, this condition is well satisfied for $a > 0.2$ μm, i.e., not restrictive.

The reflection coefficient (13) can be identically rewritten in the form

$$r_{\mathrm{TM}}(0,y) = 1 - \frac{2y}{\widetilde{\Pi}_{00,0}(y) + 2y}. \tag{19}$$

As is seen from (14), the parameter in (18) stands in front of the second contribution to $\widetilde{\Pi}_{00,0}$ by making it much larger than unity. Note that this contribution does not depend on y. Simultaneously, the main contribution to (12) is given by $y \sim 1$. Because of this, one can replace y with unity in the denominator of (19) and neglect by 2 in comparison with $\widetilde{\Pi}_{00,0}$. As a result, (19) takes the form

$$r_{\mathrm{TM}}(0,y) \approx 1 - \frac{2y}{\widetilde{\Pi}_{00,0}(1)}. \tag{20}$$

Substituting (20) into (12) and integrating with respect to y, one obtains the following asymptotic expression:

$$F_0^{as}(a,T) \approx -\frac{3k_BT\alpha_0}{4a^4}\left[1 - \frac{8}{\widetilde{\Pi}_{00,0}(1)}\right] = F_0^{\mathrm{IM}}(a,T)\left[1 - \frac{8}{\widetilde{\Pi}_{00,0}(1)}\right], \tag{21}$$

where $F_0^{\rm IM}$ is the Casimir–Polder force from an ideal metal plane at large separations defined in (17). Note that $F_0^{as}(a,T)$ depends on the Planck constant $\hbar$ through the polarization tensor of graphene $\widetilde{\Pi}_{00,0}(1)$.

Now we deal with the asymptotic expressions for the polarization tensor $\widetilde{\Pi}_{00,0}(1)$ and start from the case $\Delta=0$, $\mu\neq 0$. In this case, we have from (15) $D_0=0$ and from (8) $\Psi(0)=\pi$. Because of this, (14) simplifies to

$$\widetilde{\Pi}_{00,0}(1)\approx\frac{\alpha\pi}{\tilde{v}_F}+\frac{8\alpha k_BT}{\tilde{v}_F^2\hbar\omega_c}\ln\left[\left(1+e^{\frac{\mu}{k_BT}}\right)\left(1+e^{-\frac{\mu}{k_BT}}\right)\right]$$
$$-\frac{4\alpha}{\tilde{v}_F}\int\limits_0^1 du\left(\frac{1}{e^{B_0u+\frac{\mu}{k_BT}}+1}+\frac{1}{e^{B_0u-\frac{\mu}{k_BT}}+1}\right)\sqrt{1-u^2}. \tag{22}$$

Owing to the condition (18), the first contribution on the right-hand side of (22) is much less than the second and can be neglected. Owing to the same condition, according to (15),

$$B_0=0=\frac{\hbar c\tilde{v}_Fy}{4ak_BT}\approx\frac{\tilde{v}_F\hbar\omega_c}{2k_BT}\ll 1. \tag{23}$$

Because of this, it holds that $B_0u\ll 1$ and one can put $\exp(B_0u)\approx 1$ into (22). As a result, (22) takes the form

$$\widetilde{\Pi}_{00,0}(1)\approx\frac{8\alpha k_BT}{\tilde{v}_F^2\hbar\omega_c}\ln\left[\left(1+e^{\frac{\mu}{k_BT}}\right)\left(1+e^{-\frac{\mu}{k_BT}}\right)\right]$$
$$-\frac{4\alpha}{\tilde{v}_F}\left[\left(1+e^{\frac{\mu}{k_BT}}\right)^{-1}+\left(1+e^{-\frac{\mu}{k_BT}}\right)^{-1}\right]\int\limits_0^1 du\sqrt{1-u^2}. \tag{24}$$

Calculating the integral, we find an expression

$$\widetilde{\Pi}_{00,0}(1)\approx\frac{\alpha}{\tilde{v}_F}\left\{\frac{8k_BT}{\tilde{v}_F\hbar\omega_c}\ln\left[\left(1+e^{\frac{\mu}{k_BT}}\right)\left(1+e^{-\frac{\mu}{k_BT}}\right)\right]\right.$$
$$\left.-\pi\left[\left(1+e^{\frac{\mu}{k_BT}}\right)^{-1}+\left(1+e^{-\frac{\mu}{k_BT}}\right)^{-1}\right]\right\}, \tag{25}$$

where, thanks to (18), the second term is much less than the first. As a result, one obtains

$$\widetilde{\Pi}_{00,0}(1)\approx\frac{8\alpha k_BT}{\tilde{v}_F^2\hbar\omega_c}\ln\left[\left(1+e^{\frac{\mu}{k_BT}}\right)\left(1+e^{-\frac{\mu}{k_BT}}\right)\right]. \tag{26}$$

In the special case of a pristine graphene $\Delta=\mu=0$, (26) reduces to

$$\widetilde{\Pi}_{00,0}(1)\approx\frac{16\alpha k_BT}{\tilde{v}_F^2\hbar\omega_c}\ln 2, \tag{27}$$

which agrees with [81].

We are now coming to the case of arbitrary, but not too small, values of Δ and any value of μ. In fact, we assume that D_0 defined in (15) with $y=1$ is much larger than unity

$$D_0=\frac{2a\Delta}{\hbar c\tilde{v}_Fy}\approx\frac{\Delta}{\hbar\omega_c\tilde{v}_F}\gg 1. \tag{28}$$

The assumption in (28) is not too restrictive. The point is that we consider the Casimir–Polder force at large separations $a>2$ μm, i.e., $\hbar\omega_c<0.05$ eV. This means that the condition (28) is satisfied for all $\Delta>0.001$ eV.

Let us consider the first term in the polarization tensor (14) with $y = 1$. Using the definition of Ψ in (8) and expanding arctan (D_0^{-1}) in powers of small parameter D_0^{-1}, we obtain

$$\Psi(D_0) \approx \frac{8}{3D_0}, \qquad \frac{\alpha}{\tilde{v}_F}\Psi(D_0) \approx \frac{8\alpha}{3\tilde{v}_F D_0} = \frac{8\alpha}{3}\frac{\hbar\omega_c}{\Delta}. \tag{29}$$

The maximum value of the latter quantity in (29) (i.e., of the first term in (14)) for our values of parameters is unity, and it decreases with increasing Δ. Thus, thanks to (18), the first term in (14) is much less than the second one containing the logarithm function.

We turn our attention to the third term in (14). Due to (28), the lower and upper integration limits are very close, and one can replace $B_0 u$ with $B_0 D_0$ in the powers of exponents entering $w_0(u, y)$ defined in (9). Taking into account that, according to (15), $B_0 D_0 = \Delta/(2k_B T)$, we can rewrite (14) with $y = 1$ in the form

$$\widetilde{\Pi}_{00,0}(1) \approx \frac{8\alpha k_B T}{\tilde{v}_F^2 \hbar\omega_c} \ln\left[\left(e^{-\frac{\Delta}{2k_B T}} + e^{\frac{\mu}{k_B T}}\right)\left(e^{-\frac{\Delta}{2k_B T}} + e^{-\frac{\mu}{k_B T}}\right)\right] \tag{30}$$

$$-\frac{4\alpha}{\tilde{v}_F}\left(\frac{1}{e^{\frac{\Delta}{2k_B T}+\frac{\mu}{k_B T}}+1} + \frac{1}{e^{\frac{\Delta}{2k_B T}-\frac{\mu}{k_B T}}+1}\right)\int\limits_{D_0}^{\sqrt{1+D_0^2}} du \frac{1-u^2}{\sqrt{1-u^2+D_0^2}}.$$

The integral in (30) is easily calculated

$$I = \int\limits_{D_0}^{\sqrt{1+D_0^2}} du \frac{1-u^2}{\sqrt{1-u^2+D_0^2}} = -\frac{D_0}{2} + \frac{D_0^2-1}{2}\left(\arctan D_0 - \frac{\pi}{2}\right). \tag{31}$$

Under the condition (28), we find from (31) $I \approx -D_0$ and (30) leads to

$$\widetilde{\Pi}_{00,0}(1) \approx \frac{8\alpha k_B T}{\tilde{v}_F^2 \hbar\omega_c} \ln\left[\left(e^{-\frac{\Delta}{2k_B T}} + e^{\frac{\mu}{k_B T}}\right)\left(e^{-\frac{\Delta}{2k_B T}} + e^{-\frac{\mu}{k_B T}}\right)\right]$$

$$+\frac{4\alpha\Delta}{\tilde{v}_F^2 \hbar\omega_c}\left(\frac{1}{e^{\frac{\Delta}{2k_B T}+\frac{\mu}{k_B T}}+1} + \frac{1}{e^{\frac{\Delta}{2k_B T}-\frac{\mu}{k_B T}}+1}\right). \tag{32}$$

After making identical transformations in the first and second terms of this expression, we bring it to the form (see (A7) in Appendix A for details)

$$\widetilde{\Pi}_{00,0}(1) \approx \frac{8\alpha k_B T}{\tilde{v}_F^2 \hbar\omega_c}\left[\ln\left(4\cosh\frac{\Delta+2\mu}{4k_B T}\cosh\frac{\Delta-2\mu}{4k_B T}\right)\right.$$

$$\left.-\frac{\Delta}{4k_B T}\left(\tanh\frac{\Delta+2\mu}{4k_B T} + \tanh\frac{\Delta-2\mu}{4k_B T}\right)\right]. \tag{33}$$

By putting $\mu = 0$ in (33), one finds

$$\widetilde{\Pi}_{00,0}(1) \approx \frac{16\alpha k_B T}{\tilde{v}_F^2 \hbar\omega_c}\left[\ln\left(2\cosh\frac{\Delta}{4k_B T}\right) - \frac{\Delta}{4k_B T}\tanh\frac{\Delta}{4k_B T}\right]. \tag{34}$$

Under the additional condition $\Delta \ll 4k_B T$, we can neglect the second term in (34), as compared to the first one, and obtain

$$\widetilde{\Pi}_{00,0}(1) \approx \frac{16\alpha k_B T}{\tilde{v}_F^2 \hbar\omega_c}\ln\left(2\cosh\frac{\Delta}{4k_B T}\right). \tag{35}$$

This result coincides with that obtained earlier in [81] if it is taken into account that [81] uses the notation $\tilde{\Delta} = \Delta/(\hbar\omega_c)$, where Δ is equal to $\Delta/2$ in our current notations, i.e., to one-half of the total energy gap.

Note that at $T = 300$ K the application region of (35) reduces to 0.001 eV $< \Delta <$ 0.01 eV, i.e., it is rather narrow. In Appendix A, using the condition opposite to (28), we prove, however, that (35) remains valid for arbitrary small values of Δ (see Equation (A8) with any μ including $\mu = 0$).

Now we finalize the asymptotic expression F_0^{as} for the Casimir–Polder force from gapped and doped graphene with not-too-small energy gaps Δ. For this purpose, we substitute (33) into (21). The obtained expression F_0^{as} is valid under the condition (18). In the next section, we find how close the asymptotic Casimir–Polder force would be to the numerical values of the force at large separations F_0.

5. Comparison between Asymptotic and Numerical Results

Here, we compare the analytic asymptotic expressions for the large-separation Casimir–Polder force, F_0^{as}, obtained in Section 4 with numerical computations of F_0 for different values of the energy gap and chemical potential.

We begin with the case of an undoped graphene sheet, $\mu = 0$, and calculate the ratio F_0/F_0^{as} for different values of the energy gap Δ. In doing so, F_0 is computed by (12)–(15) and F_0^{as} by (21) and (34). All computations are performed at $T = 300$ K.

In Figure 3, the ratio F_0/F_0^{as} is shown as a function of separation between an atom (nanoparticle) and a graphene sheet by the three lines counted from top to bottom for the energy gap Δ = 0.1, 0.15, and 0.2 eV. The case of large separations up to 100 μm is shown in the inset for Δ = 0.15 and 0.2 eV.

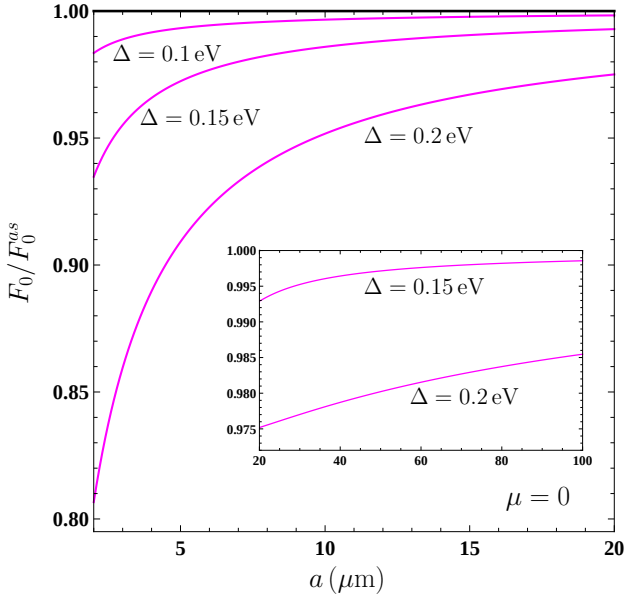

Figure 3. The ratio of the Casimir–Polder force from a graphene sheet with $\mu = 0$ at large separations to its asymptotic behavior is shown as a function of separation by the three lines counted from top to bottom for energy gap Δ equal to 0.1, 0.15, and 0.2 eV. In the inset, the two lines for $\Delta = 0.15$ and 0.2 eV are shown at larger separations.

As can be seen in Figure 3, the best agreement between the asymptotic and computed Casimir–Polder forces holds for the smallest Δ = 0.1 eV. In this case, F_0^{as} agrees with F_0 in the limits of 1% at any $a > 3$ μm. With increasing Δ, the agreement between F_0^{as} and F_0 becomes worse. Thus, for a graphene sheet with Δ = 0.15 eV, the 1% agreement is reached at a = 14 μm. As for graphene with Δ = 0.2 eV, the 2% agreement is only reached at a = 50 μm.

Now we consider the impact of the chemical potential on the measure of agreement between F_0^{as} and F_0. For this purpose, we consider graphene sheets with Δ = 0.2 eV (the case of the worst agreement in Figure 3) but various values of chemical potential. Computations of F_0^{as} are performed by (21) and (33).

In Figure 4, the ratio F_0/F_0^{as} is again shown as a function of separation by the three lines counted from top to bottom for chemical potentials $\mu = 150$, 75, and 25 meV, respectively (brown, blue, and red lines). In the inset, the lines for a graphene sheet with $\mu = 75$ and 25 meV are shown in the region of large separations up to 100 μm.

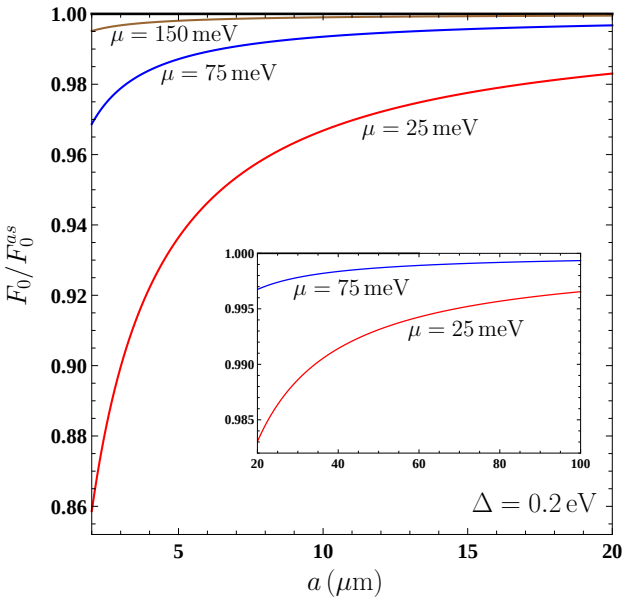

Figure 4. The ratio of the Casimir–Polder force from a graphene sheet with $\Delta = 0.2$ eV at large separations to its asymptotic behavior is shown as a function of separation by the three lines counted from top to bottom for chemical potential μ equal to 150, 75, and 25 meV. In the inset, the two lines for $\mu = 75$ and 25 meV are shown at larger separations.

From Figure 4, one can conclude that an increase in the value of the chemical potential makes the agreement between F_0^{as} and F_0 better. Thus, for $\mu = 150$ meV, the 1% agreement occurs at all separations $a > 3$ μm, whereas for $\mu = 75$ meV, at $a > 5.5$ μm. For a graphene sheet with $\mu = 25$ meV the 1% agreement is reached only at $a \approx 34$ μm. We can say that an increase in the values of Δ and μ acts on the agreement between F_0^{as} and F_0 in opposite directions by making it worse and better, respectively, at the same separation distance.

The above results allow the determination of the region of distances where the large-separation Casimir-Polder force F_0 can be replaced with its asymptotic behavior F_0^{as} depending on the values of the energy gap and chemical potential of the specific graphene sheet. These results are valid for both light and heavy atoms and for spherical nanoparticles.

6. Discussion

As discussed in Section 1, the Casimir–Polder force on atoms and nanoparticles from different surfaces, including graphene, has been the subject of topical investigations in the interests of fundamental physics and its applications. The Casimir–Polder force from graphene attracts special attention because graphene is a novel material of high promise due to its unusual mechanical and electrical properties.

From a theoretical point of view, graphene offers major advantages over more conventional materials because its response functions to the electromagnetic field can be found on the basis of the first principles of thermal quantum field theory without resorting to phenomenological models. This is not the case for real metals, the response of which to low-frequency electromagnetic field is described by the phenomenological Drude model, which lacks an experimental confirmation in the area of s-polarized evanescent waves giving an important contribution to the Casimir effect [82,83]. As a result, there are contradictions between the predictions of the Lifshitz theory and measurements of the Casimir force between metallic surfaces (see [77,80,84,85] for a review).

Although the Casimir–Polder force from graphene has not yet been measured, the already performed measurements of the Casimir force between a graphene-coated plate and a Au-coated sphere demonstrate excellent agreement between the theoretical predictions of the Lifshitz theory using the polarization tensor of graphene and the measurement data [86,87]. Because of this, the above results for the Casimir–Polder force from gapped and doped graphene at large separations, obtained here using the formalism of the polarization tensor, are of a high degree of reliability.

7. Conclusions

To conclude, in the foregoing we investigated the Casimir–Polder force acting on atoms and nanoparticles from a gapped and doped graphene sheet at large separations. We have found separation distances, starting from which the zero-frequency term of the Lifshitz formula coincides with the total Casimir–Polder force acting on heavy atoms or spherical nanoparticles in the limits of 1%. It was shown that, depending on the values of the energy gap and chemical potential of graphene, the classical limit may be reached at much larger distances than the limit of large separations.

Furthermore, we derived the analytic asymptotic expressions for the zero-frequency term of the Lifshitz formula at large separations with the reflection coefficient expressed via the polarization tensor of graphene. These expressions are valid for light and heavy atoms and nanoparticles of spherical shape. The obtained asymptotic expressions were compared with numerical computations of the zero-frequency term. According to our results, with the increasing energy gap of graphene, the separation distance ensuring a better than 1% agreement between the asymptotic and numerically computed forces also increases. By contrast, an increase in the chemical potential of graphene leads to a 1% agreement between the asymptotic and numerical results at shorter separations.

The obtained results make it possible to easily calculate the large-separation Casimir–Polder force from the gapped and doped graphene sheets and to control it by varying the values of the energy gap and chemical potential. This can be used in precision experiments on quantum reflection and Bose–Einstein condensation near the surfaces of graphene, as well as in various technological applications. In the future, it would be interesting to investigate the large-separation Casimir–Polder force from graphene-coated substrates made of different materials.

Author Contributions: Conceptualization, G.L.K. and V.M.M.; investigation, G.L.K. and V.M.M.; writing—original draft, V.M.M.; writing—review and editing, G.L.K. All authors have read and agreed to the published version of the manuscript.

Funding: G.L.K. was partially funded by the Ministry of Science and Higher Education of the Russian Federation (The World-Class Research Center: Advanced Digital Technologies, contract no. 075-15-2022-311, dated 20 April 2022). The research of V.M.M. was partially carried out in accordance with the Strategic Academic Leadership Program Priority 2030 of the Kazan Federal University.

Institutional Review Board Statement: Not applicable.

Informed Consent Statement: Not applicable.

Data Availability Statement: Not applicable.

Conflicts of Interest: The authors declare no conflict of interest.

Appendix A. Asymptotic Expression for Graphene with Small Energy Gap

The asymptotic expression for the Casimir–Polder force from gapped and doped graphene obtained in Section 4 is valid for graphene satisfying the condition (28), i.e., having not too small energy gap. Here, we consider the separation region where the condition (18) is again satisfied but the energy gap satisfies the condition

$$D_0 \approx \frac{\Delta}{\tilde{v}_F \hbar \omega_c} \ll 1, \tag{A1}$$

which is just the opposite to (28).

Owing the condition (18), the inequality in (23) preserves its validity and the first contribution to the polarization tensor (14) with $y = 1$ is much less than the second and can be omitted.

First, we evaluate the third contribution to (14) given by

$$I(1) = -\frac{4\alpha}{\tilde{v}_F}\int\limits_{D_0}^{\sqrt{1+D_0^2}} du\left(\frac{1}{e^{B_0 u+\frac{\mu}{k_BT}}+1}+\frac{1}{e^{B_0 u-\frac{\mu}{k_BT}}+1}\right)\frac{1-u^2}{\sqrt{1-u^2+D_0^2}}. \tag{A2}$$

By introducing the new integration variable $v = u - D_0$, this term takes the form

$$I(1) = -\frac{4\alpha}{\tilde{v}_F}\int\limits_{0}^{\sqrt{1+D_0^2}-D_0} dv\left(\frac{1}{e^{\frac{\Delta}{2k_BT}+\frac{\mu}{k_BT}}e^{B_0 v}+1}+\frac{1}{e^{\frac{\Delta}{2k_BT}-\frac{\mu}{k_BT}}e^{B_0 v}+1}\right)$$
$$\times\left(\sqrt{1-v^2-2vD_0}-\frac{D_0^2}{\sqrt{1-v^2-2vD_0}}\right). \tag{A3}$$

Using (A1), we conclude that the upper integration limit in (A3) is $\sqrt{1+D_0^2}-D_0 \sim 1$. Then, because of (23), one can put $\exp(B_0 v) \approx 1$ and rewrite (A3) as

$$I(1) \approx -\frac{4\alpha}{\tilde{v}_F}\left(\frac{1}{e^{\frac{\Delta}{2k_BT}+\frac{\mu}{k_BT}}+1}+\frac{1}{e^{\frac{\Delta}{2k_BT}-\frac{\mu}{k_BT}}+1}\right)$$
$$\times\int\limits_{0}^{\sqrt{1+D_0^2}-D_0} dv\left(\sqrt{1-v^2-2vD_0}-\frac{D_0^2}{\sqrt{1-v^2-2vD_0}}\right). \tag{A4}$$

Calculating the integral in (A4), we obtain

$$I(1) \approx -\frac{2\alpha}{\tilde{v}_F}\left(\frac{1}{e^{\frac{\Delta}{2k_BT}+\frac{\mu}{k_BT}}+1}+\frac{1}{e^{\frac{\Delta}{2k_BT}-\frac{\mu}{k_BT}}+1}\right)$$
$$\times\left[(1-D_0^2)\frac{\pi}{2}-D_0-(1+D_0^2)\mathrm{arctan}D_0\right] \tag{A5}$$
$$=-\frac{2\alpha}{\tilde{v}_F}\left(\frac{1}{e^{\frac{\Delta}{2k_BT}+\frac{\mu}{k_BT}}+1}+\frac{1}{e^{\frac{\Delta}{2k_BT}-\frac{\mu}{k_BT}}+1}\right)[\pi+O(D_0)].$$

Taking into account (18), it can be seen that the magnitude of $I(1)$ is much less than the second term in the polarization tensor (14) and can be omitted.

Thus, we are left with only the second term in (14)

$$\widetilde{\Pi}_{00,0}(1) \approx \frac{8\alpha k_BT}{\tilde{v}_F^2\hbar\omega_c}\ln\left[\left(e^{-\frac{\Delta}{2k_BT}}+e^{\frac{\mu}{k_BT}}\right)\left(e^{-\frac{\Delta}{2k_BT}}+e^{-\frac{\mu}{k_BT}}\right)\right], \tag{A6}$$

which can be transformed similarly to (32). Here, we present this transformation in greater detail

$$\widetilde{\Pi}_{00,0}(1) \approx \frac{8\alpha k_BT}{\tilde{v}_F^2\hbar\omega_c}\ln\left[e^{\frac{\mu}{k_BT}}\left(e^{-\frac{\Delta}{2k_BT}-\frac{\mu}{k_BT}}+1\right)e^{-\frac{\mu}{k_BT}}\left(e^{-\frac{\Delta}{2k_BT}+\frac{\mu}{k_BT}}+1\right)\right]$$
$$=\frac{8\alpha k_BT}{\tilde{v}_F^2\hbar\omega_c}\ln\left[e^{-\frac{\Delta+2\mu}{4k_BT}}\left(e^{\frac{\Delta+2\mu}{4k_BT}}+e^{-\frac{\Delta+2\mu}{4k_BT}}\right)e^{-\frac{\Delta-2\mu}{4k_BT}}\left(e^{\frac{\Delta-2\mu}{4k_BT}}+e^{-\frac{\Delta-2\mu}{4k_BT}}\right)\right]$$
$$=\frac{8\alpha k_BT}{\tilde{v}_F^2\hbar\omega_c}\ln\left(4\cosh\frac{\Delta+2\mu}{4k_BT}\cosh\frac{\Delta-2\mu}{4k_BT}\right)-\frac{2\alpha\Delta}{\tilde{v}_F^2\hbar\omega_c}. \tag{A7}$$

Owing to the condition (A1), the last term in (A7) can be neglected and, as a result,

$$\widetilde{\Pi}_{00,0}(1) \approx \frac{8\alpha k_B T}{\tilde{v}_F^2 \hbar\omega_c} \ln\left(4\cosh\frac{\Delta+2\mu}{4k_B T}\cosh\frac{\Delta-2\mu}{4k_B T}\right). \tag{A8}$$

For $\mu = 0$, (A8) reduces to (35). Thus, (35) is really valid for arbitrarily small Δ satisfying the condition (A1).

References

1. Casimir, H.B.G.; Polder, D. The influence of retardation on the London-van der Waals forces. *Phys. Rev.* **1948**, *73*, 360–372. [CrossRef]
2. Lifshitz, E.M. The theory of molecular attractive forces between solids. *Zh. Eksp. Teor. Fiz.* **1955**, *29*, 94–110; Translated in *Sov. Phys. JETP* **1956**, *2*, 73–83.
3. Dzyaloshinskii, I.E.; Lifshitz, E.M.; Pitaevskii, L.P. The general theory of van der Waals forces. *Usp. Fiz. Nauk* **1961**, *73*, 381–422; Translated: *Adv. Phys.* **1961**, *10*, 165–209. [CrossRef]
4. Lifshitz, E.M.; Pitaevskii, L.P. *Statistical Physics, Part II*; Pergamon: Oxford, UK, 1980.
5. Babb, J.F.; Klimchitskaya, G.L.; Mostepanenko, V.M. Casimir-Polder interaction between an atom and a cavity wall under the influence of real conditions. *Phys. Rev. A* **2004**, *70*, 042901. [CrossRef]
6. Caride, A.O.; Klimchitskaya, G.L.; Mostepanenko, V.M.; Zanette, S.I. Dependences of the van der Waals atom-wall interaction on atomic and material properties. *Phys. Rev. A* **2005**, *71*, 042901. [CrossRef]
7. Babb, J.F. Long-range atom-surface interactions for cold atoms. *J. Phys. Conf. Ser.* **2005**, *19*, 1. [CrossRef]
8. Mostepanenko, V.M.; Babb, J.F.; Caride, A.O.; Klimchitskaya, G.L.; Janette, S.I. Dependence of the Casimir-Polder interaction between atom and a cavity wall on atomic and material properties. *J. Phys. A Math. Gen.* **2006**, *39*, 6583–6588. [CrossRef]
9. Safari, H.; Welsch, D.-G.; Buhmann, S.Y.; Scheel, S. van der Waals potentials of paramagnetic atoms. *Phys. Rev. A* **2008**, *78*, 062901. [CrossRef]
10. Bimonte, G.; Klimchitskaya, G.L.; Mostepanenko, V.M. Impact of magnetic properties on atom-wall interactions. *Phys. Rev. A* **2009**, *79*, 042906. [CrossRef]
11. Haakh, H.; Intravaia, F.; Henkel, C.; Spagnolo, S.; Passante, R.; Power, B.; Sols, F. Temperature dependence of the magnetic Casimir-Polder interaction. *Phys. Rev. A* **2009**, *80*, 062905. [CrossRef]
12. Ellingsen, S.Å.; Buhmann, S.Y.; Scheel, S. Temperature-Independent Casimir-Polder Forces Despite Large Thermal Photon Numbers. *Phys. Rev. Lett.* **2010**, *104*, 223003. [CrossRef]
13. Passante, R.; Rizzuto, L.; Spagnolo, S.; Tanaka, S.; Petrosky, T.Y. Harmonic oscillator model for the atom-surface Casimir-Polder interaction energy. *Phys. Rev. A* **2012**, *85*, 062109. [CrossRef]
14. Kysylychyn, D.; Piatnytsia, V.; Lozovski, V. Electrodynamic interaction between a nanoparticle and the surface of a solid. *Phys. Rev. E* **2013**, *88*, 052403. [CrossRef]
15. Sun, W. Interaction forces between a spherical nanoparticle and a flat surface. *Phys. Chem. Chem. Phys.* **2014**, *16*, 5846–5854. [CrossRef]
16. Khusnutdinov, N.; Kashapov, R.; Woods, L.M. Casimir-Polder effect for a stack of conductive planes. *Phys. Rev. A* **2016**, *94*, 012513. [CrossRef]
17. Fuchs, S.; Crosse, J.A.; Buhmann, S.Y. Casimir-Polder shift and decay rate in the presence of nonreciprocal media. *Phys. Rev. A* **2017**, *95*, 023805. [CrossRef]
18. Fuchs, S.; Bennett, R.; Krems, R.V.; Buhmann, S.Y. Nonadditivity of Optical and Casimir-Polder Potentials. *Phys. Rev. Lett.* **2018**, *121*, 083603. [CrossRef]
19. Bordag, M.; Klimchitskaya, G.L.; Mostepanenko, V.M. Nonperturbative theory of atom-surface interaction: Corrections at short separations. *J. Phys. Condens. Matter* **2018**, *30*, 055003. [CrossRef]
20. Garcion, C.; Fabre, N.; Bricha, H.; Perales, F.; Scheel, S.; Ducloy, M.; Dutier, G. Intermediate-Range Casimir-Polder Interaction Probed by High-Order Slow Atom Diffraction. *Phys. Rev. Lett.* **2021**, *127*, 170402. [CrossRef]
21. Nayak, V.U.; Edwards, D.O.; Masuhara, N. Scattering of ^{4}He Atoms Grazing the Liquid- ^{4}He Surface. *Phys. Rev. Lett.* **1983**, *50*, 990–993. [CrossRef]
22. Berkhout, J.J.; Luiten, O.J.; Setija, I.D.; Hijmans, T.W.; Mizusaki, T.; Walraven, J.T.M. Quantum reflection: Focusing of hydrogen atoms with a concave mirror. *Phys. Rev. Lett.* **1989**, *63*, 1689–1693. [CrossRef] [PubMed]
23. Doyle, J.M.; Sandberg, J.C.; Yu, I.A.; Cesar, C.L.; Kleppner, D.; Greytak, T.J. Hydrogen in the submillikelvin regime: Sticking probability on superfluid ^{4}He. *Phys. Rev. Lett.* **1991**, *67*, 603–607. [CrossRef] [PubMed]
24. Yu, I.A.; Doyle, M.J.; Sandberg, J.C.; Cesar, C.L.; Kleppner, D.; Greytak, T.J. Evidence for universal quantum reflection of hydrogen from liquid ^{4}He. *Phys. Rev. Lett.* **1993**, *71*, 1589–1593. [CrossRef] [PubMed]
25. Shimizu, F. Specular Reflection of Very Slow Metastable Neon Atoms from a Solid Surface. *Phys. Rev. Lett.* **2001**, *86*, 987–991. [CrossRef]
26. Friedrich, H.; Jacoby, G.; Meister, C.J. Quantum reflection by Casimir-van der Waals potential tails. *Phys. Rev. A* **2002**, *65*, 032902. [CrossRef]

27. Druzhinina, V.; DeKieviet, M. Experimental Observation of Quantum Reflection far from Threshold. *Phys. Rev. Lett.* **2003**, *91*, 193202. [CrossRef]
28. Oberst, H.; Tashiro, Y.; Shimizu, K.; Shimizu F. Quantum reflection of He^* on silicon. *Phys. Rev. A* **2005**, *71*, 052901. [CrossRef]
29. Rojas-Lorenzo, G.; Rubayo-Soneira, J.; Miret-Artés, S.; Pollak, E. Influence of realistic atom wall potentials in quantum reflection traps. *Phys. Rev. A* **2007**, *75*, 022902.
30. Bezerra, V.B.; Klimchitskaya, G.L.; Mostepanenko, V.M.; Romero, C. Lifshitz theory of atom-wall interaction with applications to quantum reflection. *Phys. Rev. A* **2008**, *78*, 042901. [CrossRef]
31. Harber, D.M.; McGuirk, J.M.; Obrecht, J.M.; Cornell, E.A. Thermally Induced Losses in Ultra-Cold Atoms Magnetically Trapped Near Room-Temperature Surfaces. *J. Low Temp. Phys.* **2003**, *133*, 229–238. [CrossRef]
32. Leanhardt, A.E.; Shin, Y.; Chikkatur, A.P.; Kielpinski, D.; Ketterle, W.; Pritchard, D.E. Bose–Einstein Condensates Near a Microfabricated Surface. *Phys. Rev. Lett.* **2003**, *90*, 100404. [CrossRef]
33. Antezza, M.; Pitaevskii, L.P.; Stringari, S. Effect of the Casimir-Polder force on the collective oscillations of a trapped Bose–Einstein condensate. *Phys. Rev. A* **2004**, *70*, 053619. [CrossRef]
34. Lin, Y.-j.; Teper, I.; Chin, C.; Vuletić, V. Impact of the Casimir-Polder Potential and Johnson Noise on Bose–Einstein Condensate Stability Near Surfaces. *Phys. Rev. Lett.* **2004**, *92*, 050404. [CrossRef]
35. Harber, D.M.; Obrecht, J.M.; McGuirk, J.M.; Cornell, E.A. Measurement of the Casimir-Polder force through center-of-mass oscillations of a Bose–Einstein condensate. *Phys. Rev. A* **2005**, *72*, 033610. [CrossRef]
36. Henkel, C.; Joulain, K; Mulet, J.P.; Greffet, J.J. Radiation forces on small particles in thermal near fields. *J. Opt. A Pure Appl. Opt.* **2002**, *4*, S109–S114. [CrossRef]
37. Antezza, M.; Pitaevskii, L.P.; Stringari, S. New Asymptotic Behavior of the Surface-Atom Force out of Thermal Equilibrium. *Phys. Rev. Lett.* **2005**, *95*, 113202. [CrossRef]
38. Antezza, M.; Pitaevskii, L.P.; Stringari, S.; Svetovoy, V.B. Casimir-Lifshitz force out of thermal equilibrium. *Phys. Rev. A* **2008**, *77*, 022901. [CrossRef]
39. Bimonte, G. Scattering approach to Casimir forces and radiative heat transfer for nanostructured surfaces out of thermal equilibrium. *Phys. Rev. A* **2009**, *80*, 042102. [CrossRef]
40. Messina, R.; Antezza, M. Scattering-matrix approach to Casimir-Lifshitz force and heat transfer out of thermal equilibrium between arbitrary bodies. *Phys. Rev. A* **2011**, *84*, 042102. [CrossRef]
41. Krüger, M.; Bimonte, G.; Emig, T.; Kardar, M. Trace formulas for nonequilibrium Casimir interactions, heat radiation, and heat transfer for arbitrary bodies. *Phys. Rev. B* **2012**, *86*, 115423. [CrossRef]
42. Obrecht, J.M.; Wild, R.J.; Antezza, M.; Pitaevskii, L.P.; Stringari, S.; Cornell, E.A. Measurement of the temperature dependence of the Casimir-Polder force. *Phys. Rev. Lett.* **2007**, *98*, 063201. [CrossRef] [PubMed]
43. Klimchitskaya, G.L.; Mostepanenko, V.M. Conductivity of dielectric and thermal atom-wall interaction. *J. Phys. A Math. Theor.* **2008**, *41*, 312002. [CrossRef]
44. Krüger, M.; Emig, T.; Bimonte, G.; Kardar, M. Non-equilibrium Casimir forces: Spheres and sphere-plate. *Europhys. Lett.* **2011**, *95*, 21002. [CrossRef]
45. Klimchitskaya, G.L.; Mostepanenko, V.M. Casimir-Polder Interaction of an Atom with a Cavity Wall Made of Phase-Change Material out of Thermal Equilibrium. *Atoms* **2020**, *9*, 4. [CrossRef]
46. Aoki, H.; Dresselhaus, M.S. (Eds.) *Physics of Graphene*; Springer: Cham, Switzerland, 2014.
47. Judd, T.E.; Scott, R.G.; Martin, A.M.; Kaczmarek, B.; Fromhold, T.M. Quantum reflection of ultracold atoms from thin films, graphene and semiconductor heterostructures. *New J. Phys.* **2011**, *13*, 083020. [CrossRef]
48. Chaichian, M.; Klimchitskaya, G.L.; Mostepanenko, V.M.; Tureanu, A. Thermal Casimir-Polder interaction of different atoms with graphene. *Phys. Rev. A* **2012**, *86*, 012515. [CrossRef]
49. Arora, B.; Kaur, H.; Sahoo, B.K. C_3 coefficients for the alkali atoms interacting with a graphene and carbon nanotube. *J. Phys. B* **2014**, *47*, 155002. [CrossRef]
50. Kaur, K.; Kaur, J.; Arora, B.; Sahoo, B.K. Emending thermal dispersion interaction of Li, Na, K and Rb alkali-metal atoms with graphene in the Dirac model. *Phys. Rev. B* **2014**, *90*, 245405. [CrossRef]
51. Klimchitskaya, G.L.; Mostepanenko, V.M. Impact of graphene coating on the atom-plate interaction. *Phys. Rev. A* **2014**, *89*, 062508. [CrossRef]
52. Cysne, T.; Kort-Kamp, W.J.M.; Oliver, D.; Pinheiro, F.A.; Rosa, F.S.S.; Farina, C. Tuning the Casimir-Polder interaction via magneto-optical effects in graphene. *Phys. Rev. A* **2014**, *90*, 052511. [CrossRef]
53. Kaur, K.; Arora, B.; Sahoo, B.K. Dispersion coefficients for the interactions of the alkali-metal and alkaline-earth-metal ions and inert-gas atoms with a graphene layer. *Phys. Rev. A* **2015**, *92*, 032704. [CrossRef]
54. Henkel, C.; Klimchitskaya, G.L.; Mostepanenko, V.M. Influence of the chemical potential on the Casimir-Polder interaction between an atom and gapped graphene or a graphene-coated substrate. *Phys. Rev. A* **2018**, *97*, 032504. [CrossRef]
55. Khusnutdinov, N.; Kashapov, R.; Woods, L.M. Thermal Casimir and Casimir-Polder interactions in N parallel 2D Dirac materials. *2D Mater.* **2018**, *5*, 035032. [CrossRef]
56. Klimchitskaya G.L.; Mostepanenko V.M. Nernst heat theorem for an atom interacting with graphene: Dirac model with nonzero energy gap and chemical potential. *Phys. Rev. D* **2020**, *101*, 116003. [CrossRef]

57. Khusnutdinov, N.; Emelianova, N. The Low-Temperature Expansion of the Casimir-Polder Free Energy of an Atom with Graphene. *Universe* **2021**, *7*, 70. [CrossRef]
58. Klimchitskaya, G.L. The Casimir-Polder interaction of an atom and real graphene sheet: Verification of the Nernst heat theorem. *Mod. Phys. Lett. A* **2020**, *35*, 2040004. [CrossRef]
59. Klimchitskaya, G.L.; Mostepanenko, V.M. Casimir and Casimir-Polder Forces in Graphene Systems: Quantum Field Theoretical Description and Thermodynamics. *Universe* **2020**, *6*, 150. [CrossRef]
60. Das, B.; Choudhury, B.; Gomathi, A.; Manna, A.K.; Pati, S.K.; Rao, C.N.R. Interaction of Inorganic Nanoparticles with Graphene. *ChemPhysChem* **2011**, *12*, 937–943. [CrossRef]
61. Biehs, S.-A.; Agarwal, G.S. Anisotropy enhancement of the Casimir-Polder force between a nanoparticle and graphene. *Phys. Rev. A* **2015**, *90*, 042510; Erratum in *Phys. Rev. A* **2015**, *91*, 039901. [CrossRef]
62. Devi, J.M. Simulation Studies on the Interaction of Graphene and Gold Nanoparticle. *Int. J. Nanosci.* **2018**, *17*, 1760043. [CrossRef]
63. Low, S.; Shon, Y.-S. Molecular interactions between pre-formed metal nanoparticles and graphene families. *Adv. Nano Res.* **2018**, *6*, 357–375. [PubMed]
64. Huang, L.-W.; Jeng, H.-T.; Su, W.-B.; Chang, C.-S. Indirect interactions of metal nanoparticles through graphene. *Carbon* **2021**, *174*, 132–137. [CrossRef]
65. Klimchitskaya, G.L.; Mostepanenko, V.M.; Tsybin, O.Y. Casimir-Polder attraction and repulsion between nanoparticles and graphene in out-of-thermal-equilibrium conditions. *Phys. Rev. B* **2022**, *105*, 195430. [CrossRef]
66. Castro Neto, A.H.; Guinea, F.; Peres, N.M.R.; Novoselov, K.S.; Geim, A.K. The electronic properties of graphene. *Rev. Mod. Phys.* **2009**, *81*, 109–162. [CrossRef]
67. Katsnelson, M.I. *The Physics of Graphene*; Cambridge University Press: Cambridge, UK, 2020.
68. Zhu, T.; Antezza, M.; Wang, J.-S. Dynamical polarizability of graphene with spatial dispersion. *Phys. Rev. B* **2021**, *103*, 125421. [CrossRef]
69. Bordag, M.; Fialkovsky, I.V.; Gitman, D.M.; Vassilevich, D.V. Casimir interaction between a perfect conductor and graphene described by the Dirac model. *Phys. Rev. B* **2009**, *80*, 245406. [CrossRef]
70. Fialkovsky, I.V.; Marachevsky, V.N.; Vassilevich, D.V. Finite-temperature Casimir effect for graphene. *Phys. Rev. B* **2011**, *84*, 035446. [CrossRef]
71. Bordag, M.; Klimchitskaya, G.L.; Mostepanenko, V.M.; Petrov, V.M. Quantum field theoretical description for the reflectivity of graphene. *Phys. Rev. D* **2015**, *91*, 045037; Erratum in *Phys. Rev. D* **2016**, *93*, 089907. [CrossRef]
72. Bordag, M.; Fialkovskiy, I.; Vassilevich, D. Enhanced Casimir effect for doped graphene. *Phys. Rev. B* **2016**, *93*, 075414; Erratum in *Phys. Rev. B* **2017**, *95*, 119905. [CrossRef]
73. Klimchitskaya, G.L.; Mostepanenko, V.M. Classical Casimir-Polder force between polarizable microparticles and thin films including graphene. *Phys. Rev. A* **2014**, *89*, 012516. [CrossRef]
74. Gusynin, V.P.; Sharapov, S.G.; Carbotte, J.P. On the universal ac optical background in graphene. *New J. Phys.* **2009**, *11*, 095013. [CrossRef]
75. Pyatkovsky, P.K. Dynamical polarization, screening, and plasmons in gapped graphene. *J. Phys. Condens. Matter* **2009**, *21*, 025506. [CrossRef]
76. Falkovsky, L.A. Optical properties of graphene. *J. Phys. Conf. Ser.* **2008**, *129*, 012004. [CrossRef]
77. Bordag, M.; Klimchitskaya, G.L.; Mohideen, U.; Mostepanenko, V.M. *Advances in the Casimir Effect*; Oxford University Press: Oxford, UK, 2015.
78. Klimchitskaya, G.L.; Mostepanenko, V.M.; Sernelius, B.E. Two approaches for describing the Casimir interaction with graphene: density-density correlation function versus polarization tensor. *Phys. Rev. B* **2014**, *89*, 125407. [CrossRef]
79. Klimchitskaya, G.L.; Mostepanenko, V.M. Quantum field theoretical framework for the electromagnetic response of graphene and dispersion relations with implications to the Casimir effect. *Phys. Rev. D* **2023**, *107*, 105007. [CrossRef]
80. Klimchitskaya, G.L.; Mohideen, U.; Mostepanenko, V.M. The Casimir force between real materials: Experiment and theory. *Rev. Mod. Phys.* **2009**, *81*, 1827–1885. [CrossRef]
81. Bordag, M.; Klimchitskaya, G.L.; Mostepanenko, V.M. Thermal Casimir effect in the interaction of graphene with dielectrics and metals. *Phys. Rev. B* **2012**, *86*, 165429. [CrossRef]
82. Klimchitskaya, G.L.; Mostepanenko, V.M.; Svetovoy, V.B. Probing the response of metals to low-frequency s-polarized evanescent waves. *Europhys. Lett.* **2022**, *139*, 66001. [CrossRef]
83. Klimchitskaya, G.L.; Mostepanenko, V.M.; Svetovoy, V.B. *Exp. Crusis* Electromagn. Response Met. Toevanescent Waves Casimir Puzzle. *Universe* **2022**, *8*, 574. [CrossRef]
84. Woods, L.M.; Dalvit, D.A.R.; Tkachenko, A.; Rodriguez-Lopez, P.; Rodriguez, A.W.; Podgornik, R. Materials perspective on Casimir and van der Waals interactions. *Rev. Mod. Phys.* **2016**, *88*, 045003. [CrossRef]
85. Mostepanenko, V.M. Casimir Puzzle and Conundrum: Discovery and Search for Resolution. *Universe* **2021**, *7*, 84. [CrossRef]

86. Liu, M.; Zhang, Y.; Klimchitskaya, G.L.; Mostepanenko, V.M.; Mohideen, U. Demonstration of Unusual Thermal Effect in the Casimir Force from Graphene. *Phys. Rev. Lett.* **2021**, *126*, 206802. [CrossRef] [PubMed]
87. Liu, M.; Zhang, Y.; Klimchitskaya, G.L.; Mostepanenko, V.M.; Mohideen, U. Experimental and theoretical investigation of the thermal effect in the Casimir interaction from graphene. *Phys. Rev. B* **2021**, *104*, 085436. [CrossRef]